Numerical Investigation of Effect of Drum Barrel on Coal-Loading Performance of Thin-Coal-Seam Shearer Machines

Xiaodi Zhang [1,2], Kuidong Gao [1,3,*], Qingliang Zeng [1,4], Lisong Lin [1], Tianjiao Wu [1] and Liqing Sun [1]

[1] College of Mechanical and Electronical Engineering, Shandong University of Science and Technology, Qingdao 266590, China; tb21050026b4@cumt.edu.cn (X.Z.); qlzeng@sdust.edu.cn (Q.Z.); lls1164905195@163.com (L.L.); wtjsdust@163.com (T.W.); slqsdust@163.com (L.S.)

[2] School of Mechatronic Engineering, China University of Mining and Technology, Xuzhou 221116, China

[3] Shandong Province Key Laboratory of Mine Mechanical Engineering, Shandong University of Science and Technology, Qingdao 266590, China

[4] School of Information Science and Engineering, Shandong Normal University, Jinan 250014, China

* Correspondence: gaokuidong22@163.com; Tel.: +86-159-5482-7709

Abstract: Thin-coal-seam shearer mining efficiency is seriously restricted by the poor loading performance of the drum. The loading of the drum to the cracked coal lumps is based on a screw-conveying mechanism, and its loading performance is influenced by many structural parameters, including drum width, helical angle, axial tilt angle, number of blades and form and diameter of the barrel. The barrel diameter directly influences the drum envelope zone's capacity, and its influence on loading performance is not yet clear. Therefore, this work first compared the drum-loading results between experiments and numerical modeling, and the results proved that the application of the discrete element method (DEM) to the modeling drum loading process is feasible and the results are reliable. Secondly, the influence of barrel diameter on particles' axial velocity, loading rate and web depth was studied using the ejection and pushing modes. The results showed that the particles' axial velocity has a noticeable impact on loading rate under ejection loading conditions, and the loading rate first increases and then decreases with the increase in barrel diameter. When the diameter is less than 700 mm in drum-pushing modes, the particles' axial velocity plays an important role on drum loading; the filling level has an obvious impact on loading performance when the barrel diameter is larger than 700 mm. The drum loading ejection rate is 25% higher than that of pushing mode, which is due to the loading rate of particles located in a web depth from 300 to 600 mm. The influence of barrel diameter on loading performance using drum ejection is more obvious than that in pushing mode. The results provide a reference for drum structural design to some extent.

Keywords: coal shearer drum; loading performance; drum barrel diameter; DEM

1. Introduction

The safe and efficient excavation of coal, as an important energy reserve and raw material for industrial production, concerns many scholars [1]. As a vital device in long wall mining, drum shearers are widely used and highly adaptable and are responsible for breaking coal and loading it onto the conveyor. The poor working environment and high working intensity of shearers result in many serious problems. Many researchers have conducted studies on the cutting performance of picks [2–4] and drums and the reliability of traction units [5–7]. Due to the widespread mining of coal due to industrialization, the reservation of thick and medium-thick coal seams, which are less difficult to mine, is gradually decreasing, and the thin coal seams with a rich reservation have attracted increasing attention. The problems in the process of mining thin coal seams cannot be neglected and include the complicated mining environment and extremely poor loading

performance caused by the small drum diameter, which restricts the efficiency of thin-coal-seam mining and threatens the safety of workers. Therefore, improvement of the loading performance of thin-coal-seam shearers has become an important issue among scholars at home and abroad [8,9].

The potential factors which impact the loading performance of thin-coal-seam shearers include structural and motion parameters. The helical angle, numbers of helical vanes, haulage speed, rotary speed of the drum and web depth were investigated and analyzed by Gao [10]. A "Globiod" drum with an exponential curve shape barrel was proposed by Ayhan [11], and it was verified that the new type drum can exponentially improve coal-loading performance using an underground practical test. Bołoz [12] proposed a single cutting head longwall shearer for the exploitation of thin coal seams, and the production data proved that the developed thin coal shearer improved the exploitation efficiency. Considering the time and cost limitations of field tests, many researchers have built coal-loading testing beds to investigate the drum's loading performance in the laboratory. Gao [10,13] investigated the minimum rotary speed without choking in the process of coal-loading using theoretical derivation and laboratory tests, and orthogonal experiments were performed to study the significance of the influencing factors. The results show that the web depth and haulage speed of the shearer have an obvious impact on coal-loading performance. Based on laboratory examinations, the effect of filling rate, worm thread angle and grain size was investigated by Wydro [14].

The development of a computer technology leading to numerical modeling has become a novel research method, characterized by its low cost and high computing efficiency, and an increasing number of researchers are favoring numerical simulations for research. To solve the problems of grain materials and granular conveying in engineering projects, Cundall [15] proposed a new modeling method, the discrete element method, to reproduce the behaviors between particles during the conveying process. Subsequently, the discrete element method (DEM) was employed in many fields of granular material conveying, including screw conveyors [16–19], pneumatics [20–22], chemical engineering [23–25] and food [19,26]. With the development of the DEM and contact models between particles, the application of the DEM is widespread, and it is involved in rock breaking [27–29].

The DEM software particle flow code (PFC3d) was first employed by Gao [30] to re-produce the coal-loading process. The shearer loading process with different dip angles in the mining direction and the faceline direction was reproduced, and its effects on coal-loading performance were investigated. In addition, he compared the results of experiments and simulations and verified the feasibility and reliability of the DEM for reproducing the coal-loading process using the drum [31]. Tian [9] and Gao [32] also investigated the effect of helical angle, drum rotating speed, shearer hauling speed and barrel shape on the behavior of coarse coal particles during the loading process. Furthermore, the effect of the auxiliary loader on the improvement in coal-loading performance was studied based on DEM modeling, which provides a new method of improving the shearer's coal-loading performance [8]. Referring to the screw conveyor, the effect of an axial inclined angle of helical vanes on particle motion behavior in the coal-loading process using the DEM was investigated [33].

The factors that impact coal-loading performance, for instance, the motion parameters and structural parameters, including helical angle, diameter and number of blades and structural form of barrel, which can be observed in Figure 1, have been investigated by many researchers. However, as the core shaft of the screw conveyor has a vital impact on the conveying performance, the effect and influence mechanism of the barrel diameter on coal-loading performance are still not clear. Consequently, in the present work, the effect of barrel diameter on coal-loading rate and the motion behaviors of coarse coal particles in loading process are explored based on a combination of experiments and DEM modeling to reveal the influence mechanism of the barrel diameter. The rest of this paper is organized as follows. In Section 2, the contact model of particles is introduced, the calibration of the main DEM parameters is outlined, the experimental apparatus is introduced and the results

of experiments and simulations are compared. The developed DEM model is also verified. The effect of barrel diameter on particle motion behaviors and the drum's coal-loading rate with ejection and pushing modes, respectively, is analyzed and discussed. Finally, the main conclusions are drawn in Section 4.
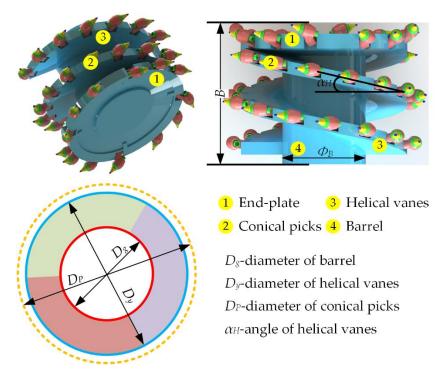

Figure 1. Main structures of cutting drum of shearer.

2. Materials and Methods

2.1. Discrete Element Method (DEM)

The aim of the DEM is to discretize the granular material into a certain number of particles, and the particles and the wall are attributed to respective properties. The particle–particle and particle–wall contact laws comply with Newton's second law and the force-displacement law. The calculation progress includes four steps: (a) initializing the position, velocity and contact information of particles and walls; (b) calculating the particle–particle and particle–wall contact force with the force-displacement law and obtaining the force and torque of particles; (c) calculating the velocities and positions of each particle based on Newton's second law; (d) updating the position, velocity and contact information of particles and walls.

The Hertz–Mindlin model and bonding-particle model were chosen from many DEM contact models as the particle–particle contact models before and after coal wall crushing, respectively. More details on the contact models are given in the next subsections.

2.1.1. Hertz–Mindlin (HM) Model

The HM model is the basic DEM model and is used to describe the particle–particle contact behavior before coal wall crushing and the particle–wall behavior. The HM model consists of spring and damping elements, and the calculation formula is given by Equation (1):

$$
\begin{cases}
F_n = \frac{4}{3} E^* \sqrt{R^*} \delta_n^{\frac{3}{2}} \\
F_t = -S_t \delta_t
\end{cases}
\tag{1}
$$

where F_n is the normal stress; δ_n is the normal overlap; E^* is the equivalent Young's modulus; R^* is the equivalent radius; F_t is the tangential stress; δ_t is the tangential overlap and S_t is the tangential stiffness.

2.1.2. Bonding-Particle (BP) Model

The BP model was first proposed by Potyondy and Cundall [34] and has been verified to reproduce the rock fracture process very well. The BP model glues the single particles as a whole block by creating a virtual chain, namely a bonded key between particles, which can sustain normal and tangential forces. The bonded key could be broken if the tensile or compression stress forced onto particles is larger than the breaking strength of the bonded key, leading the particle–particle contact model to automatically transfer from the BP model to the HM model. Hence, the BP model is used to glue single coal particles to build a coal wall, and after crushing the particle–particle contact model is changed to an HM model. The breaking criterion of the bonded key is given by Equation (2):

$$\begin{cases} F_n \geq R_n \\ F_t \geq R_t \end{cases} \tag{2}$$

where R_n is the normal strength of the bonded key; R_t is the tangential strength of the bonded key; F_n is the normal stress and F_t is the tangential stress.

2.2. Parameter Calibration

In the DEM, the numerical simulation results are affected by factors such as particle shape and mesostructured parameters, including restitution coefficient, static friction and rolling friction coefficient, which can be calibrated by rebound test, sliding test and repose angle test, respectively.

2.2.1. Particle Shape

Spherical particles are popular in the DEM due to their uncomplicated shape and high computational efficiency. However, particle motion is affected by rolling friction and sliding friction, which leads to problems as the spherical particle uses point contact. Therefore, the results with spherical particles tend to have a large rate of error, while coal particles excavated from the coal wall are not regular balls in actual working conditions. Referring to References [35,36], on the premise of ensuring the accuracy of the modeling results, the coal particle is filled in the DEM to a pyramid shape based on coal bulk excavated by a thin coal shearer, and the equivalent radius is 15 mm, as shown in Figure 2.
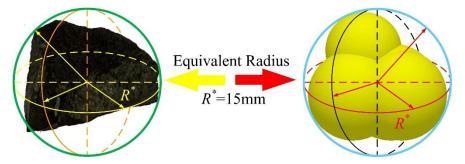

Figure 2. Coal particle filling shape in the DEM.

2.2.2. Restitution Coefficient Test

The damping element in an HM model dissipates system energy during particle–particle and particle–wall collisions, so the restitution coefficient (RC) should be determined by a rebound test [37,38]. The schematic diagram of the rebound test is shown in Figure 3, with a coal particle freefall from H_x, which is high enough to impact the fix plane with a steel material. The rebound height was H_i (i = 1,2,3 . . .), and the restitution coefficient can be obtained by H_x/H_i. To measure the rebound height accurately, the first rebound height is generally adopted for calculation, namely H_x/H_1. In the calibration of the RC, H_x equals 350 mm, and the rebound height with different RCs is shown in Figure 4.
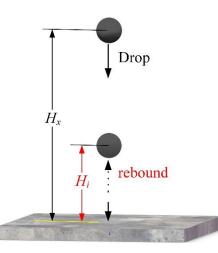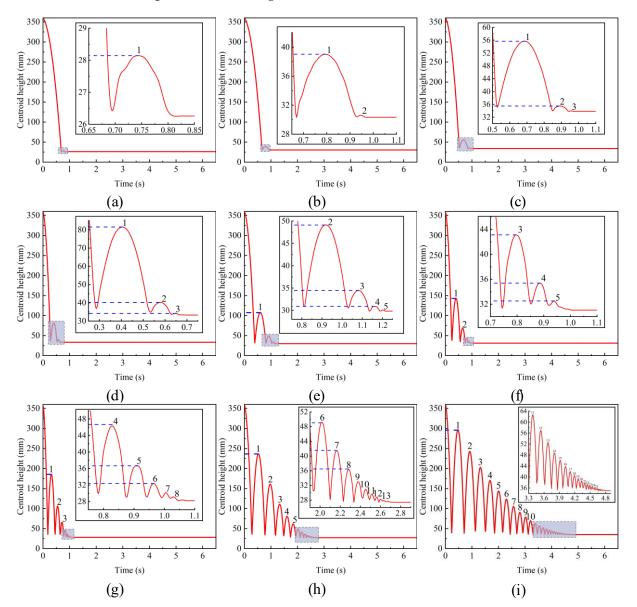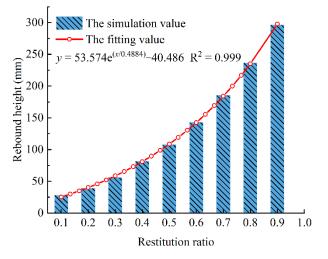
Figure 3. Schematic diagram of restitution coefficient calibration.

Figure 4. Rebound height with different RCs; (**a**) $\eta = 0.1$; (**b**) $\eta = 0.2$; (**c**) $\eta = 0.3$; (**d**) $\eta = 0.4$; (**e**) $\eta = 0.5$; (**f**) $\eta = 0.6$; (**g**) $\eta = 0.7$; (**h**) $\eta = 0.8$; (**i**) $\eta = 0.9$.

With the increase in RC, the energy dissipated in the collision between coal and steel decreased, which can be seen in Figure 4. A larger RC will lead to more bounces and a larger H_1. The relationship between the RC and H_1 is shown in Figure 5, and the exponential function can be used to describe the relationship between RC and H_1. However, the coal particle shape is irregular, and breakage will occur during the collision; these factors have an impact on the measurement results. Hence, referring to Reference [38] and combining the measurement results, the RC was determined to be 0.5 in this study, based on Figure 5.

Figure 5. Relationship between RC and H_1.

2.2.3. Sliding Test

Four typical coal particle shapes were selected in the DEM to calibrate the rolling and particle–wall sliding friction using the sliding test, as seen in Figure 6. Ball particles were selected to calibrate the rolling friction coefficient, pyramid and straight particles were selected to calibrate the rolling and sliding friction coefficient and square particles were selected to calibrate the sliding friction coefficient. The numbers of the four particle types ranged from 3 to 5, and all the particles were statically located on the horizontal steel plate. The critical rolling and static friction coefficient can be obtained by changing the gravity values in the X and Z directions of the XOZ plane. Compared with the experimental results in References [37,38], the particle–wall rolling and static friction coefficient can be obtained in the DEM.
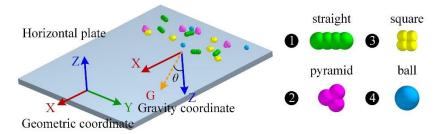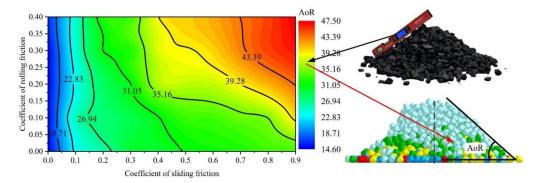

Figure 6. Sliding test in the DEM.

2.2.4. Angle of Repose (AoR) Test

The AoR test is a common method for calibrating the particle–particle friction coefficient [36]. The AoR experiments were performed repeatedly with uniform-size coal particles, which were excavated by a thin coal shearer, and the average experimental repose angle is 37.8°. In the DEM, the numerical AoR tests were performed with pyramid particles, and the numerical AoR of a combination of sliding and rolling friction, which was consistent with experimental results, was obtained and can be observed in Figure 7. The sliding and rolling frictions were 0.80 and 0.10, respectively.

Figure 7. Experimental and numerical results of AoR.

With the calibration tests for the particle shape, restitution coefficient, sliding and repose of angle, the mesoscopic particle–particle and particle–wall parameters in the DEM were obtained, as shown in Table 1.

Table 1. Material and contact parameters in the DEM.

Material	Density/kg/m^3	Poisson's Ratio	Young's Modulus/GPa
Coal	1.28×10^3	0.28	4.25
Steel	7.85×10^3	0.30	2.06×10^2
Interaction	Restitution coefficient	Sliding friction	Rolling friction
Coal–Coal	0.5	0.80	0.10
Coal–Steel	0.5	0.51	0.05

2.3. Establishment of Numerical Model

2.3.1. Establishment of Geometry Model and Coal Wall

To save computational time, only the necessary geometry models, which have an impact on simulation results, were established in the DEM, including drum, ranging arm and chain conveyor. As the stiffness of geometry is obviously larger than that of coal, and due to the geometry deformation not being considered in this study, the geometry was set as rigid in the simulation. The drum was constrained to two degrees of freedom (DOFs), including the rotational DOF in the Y direction and translation DOF in the X direction. The ranging arm had one DOF of translation in the X direction, and the chain conveyor had no DOFs. The rotary motion, drum translation and translation of the ranging arm were constant. The coal wall was built by 33,300 bonded pyramid particles, with a length, width and height of 2500, 900 and 1050 mm, respectively.

2.3.2. Division of Statistical Zone

To investigate the drum's loading performance, the distribution region of particles was divided into three areas: the drum track, namely the mined-out area whose width is equal to the drum width; the efficiency loading area, which is the groove of the chain conveyor and the gap area, which is the gap between the chain conveyor and coal wall, with a width of 100 mm. The loading rate is defined as the ratio of particle number in the effective loading area and the total number of particles excavated by the drum, which can directly reflect the drum's loading performance. The division of the statistical area is shown in Figure 8. In addition, to study the conveying performance of the drum on particles with different web depths, the coal wall was evenly divided into six sections, and the width of each section was around 150 mm.

2.4. Numerical Model Verification

The validation and feasibility of the DEM for investigating the effect of the drum barrel on loading performance was verified by coal-loading tests. The drum loading test bench is shown in Figure 9 and was composed of a hauling unit and a rotary drive unit. The drum was driven by a motor with a rotation speed of 45 rpm, and the coal wall is seen

on the moving unit, driven by a cylinder with full constraint. The hauling movement of the drum was converted into a relative movement between the drum and coal wall, and the hauling speed was set to 1 m/min. To reduce the test costs, the drum and coal wall were scaled down based on similar theories. The helical vane diameter and width of test drums were 420 and 450 mm, respectively, and the hub diameter was in the range of 150 to 240 mm with an interval of 30 mm. The distribution zone of coal particles and statistical zone is shown in Figure 10, and the statistical zone was divided into the goaf and effective loading zone. In addition, since the ranging arm has an impact on coal-loading rate, its effects were not significant compared with the drum. Hence, considering the testing costs and limitations of the test conditions, the ranging arm was not set in the tests.
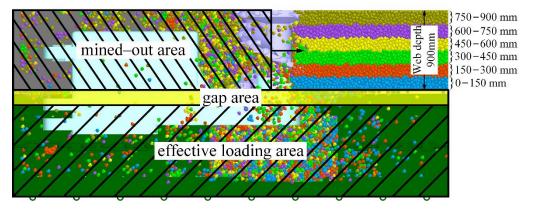

Figure 8. Division of statistical zone from top view of mining face.
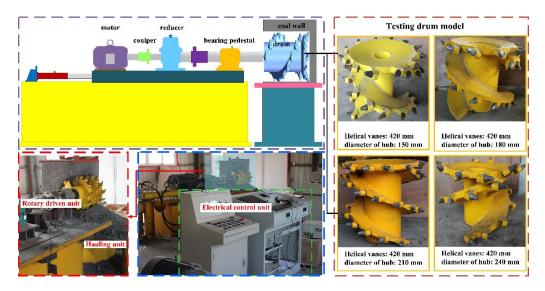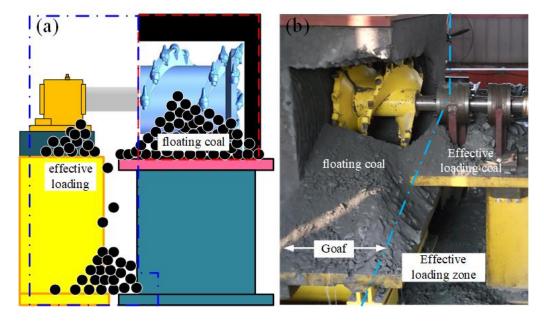

Figure 9. Coal-loading test bench.

The moving parameters of the simulated drum were consistent with the experiments. The rotary speed was set to 45 rpm, and the hauling speed was set to 1.65 m/min due to the porosity of the particles in simulation. The drums in the simulation had the same scale as practical drums, namely the helical vane diameter and width were both 900 mm, the barrel diameter was in the range of 300 to 500 mm and the interval was 50 mm. A loading rate comparison between the simulation and experiments is shown in Figure 11.

It can be seen from Figure 11 that, under ejection and pushing conditions, the changing trend of the loading rate with the ratio of the barrel diameter to blade diameter (D_g/D_y) was consistent in the DEM and tests. The loading rate in tests was notably higher than that in the DEM under both conditions because the ranging arm in simulations hindered the movement of particle flow. Another reason for this result is that the distribution zones of particles in the tests were only divided into two parts, without the gap area that exists

in the DEM. Therefore, it can be deduced that the developed model can reproduce the loading process using a drum, and the investigation of the effect of barrel diameter on loading performance and particle motion behavior was subsequently performed based on the DEM model.

Figure 10. The distribution of coal particles in coal-loading tests: (**a**) schematic diagram; (**b**) experimental distribution.
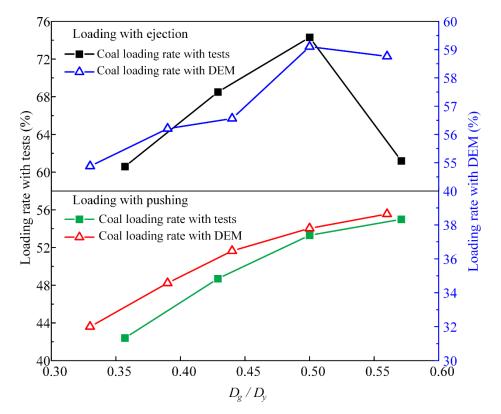

Figure 11. Comparison of loading rate between simulation and tests.
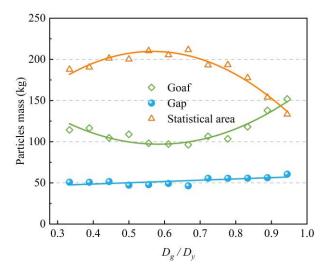
3. Results

The drum's coal-loading performance and particle motion behavior were studied and analyzed using the assessment criteria, including the distribution of particles in different

areas, axial flowing speed of particles in the drum enveloping zone, loading rate of particles located at different web depths and comprehensive drum loading rate.

3.1. The Effect of Barrel on Coal-Loading Process under Ejection Conditions

3.1.1. The Distribution of Particles in Different Areas

The distribution results of particles in different areas are shown in Figure 12. The barrel diameter has a significant effect on particle distribution in the goaf and conveyor but has no obvious impact on the gap. In addition, the barrel diameter has the opposite effect on the distribution of particles in the goaf and conveyor: with the increase in barrel diameter, the particle mass in the goaf first increases and then decreases, and the particle mass in the first goaf decreases and then increases. It should be noted that the particle mass in the goaf and conveyor increases with barrel diameter when the barrel diameter is small, and the changing range is under 25 kg; when the barrel diameter increases to 700 mm ($D_g/D_y = 0.78$), a notable increment and decrement in particle mass can be observed in the goaf and conveyor, respectively, and the changing range is more than 70 kg. With the increase in barrel diameter, the particle mass in the gap increases slightly, but this is discontinuous, which proves that there is no obvious regularity between the distribution of particles in the gap and barrel diameter.

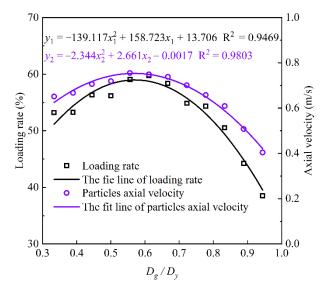**Figure 12.** Barrel diameter versus distribution of particles in ejection mode ($D_y = 900$ mm).

3.1.2. The Effect of Barrel on Loading Rate and Particles' Axial Velocity

Figure 13 shows the effect of barrel diameter on particles' axial velocity and loading rate, and their changing trend with barrel diameter is similar: a quadratic function can be used to describe the relationship. The loading rate and axial velocities first increase and then decrease with the increase in barrel diameter. When the D_g/D_y is in the range of 0.56 to 0.67, the barrel diameter is in the range of 500 to 600 mm, and the optimum axial velocities and loading rate can be obtained. The best coal-loading rate, obtained at a barrel diameter of 600 mm, is 59.7%; when the barrel diameter is 850 mm, the loading rate is the lowest, at only 38.5%. Moreover, the axial velocities of particles are apparently affected by barrel diameter, and the largest axial velocity is 0.76 m/s, which is 1.9 times the minimum. Compared to Figure 12, it can be seen that the curves of the loading rate and particle mass in the conveyor are similar, which proves that the distribution of particles in the gap area is not influenced by barrel diameter in the ejection mode.

Particles' axial velocity is an important assessment criterion to reflect the drum's conveying performance and a vital factor in the coal-loading rate. The influence of particles' axial velocity on the coal-loading rate with ejection is shown in Figure 14.

Figure 14 demonstrates that a linear function can be used to describe the relationship between coal-loading rate and particles' axial velocities, where the loading rate increases

with the increase in particles' axial velocities, which is consistent with the deduction and explains the similar changing trends of particles' axial velocities and loading rate with barrel diameter.

Figure 13. The loading rate and particles' axial velocities versus barrel diameter in ejection mode (D_y = 900 mm).
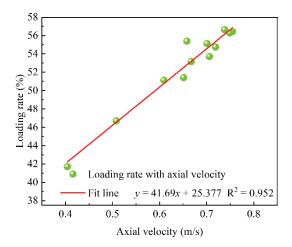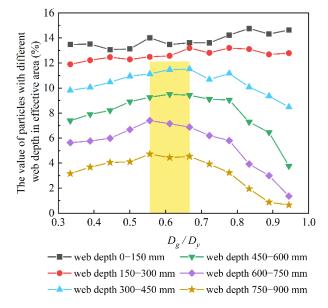

Figure 14. Particles' axial velocities versus loading rate.

3.1.3. The Effect of the Barrel on the Loading Rate of Particles with Different Web Depths

To investigate the influence mechanism of the barrel diameter on the drum's loading rate and conveying performance of particles with different web depths, the loading rates of particles with six web depths were obtained, as shown in Figure 15. In the statistical area, the loading rate of particles has an apparently linear relationship with web depths, with a smaller web depth leading to a higher particle loading rate; namely, the closer to the conveyor, the more likely the particles are to be loaded to the conveyor. When the web depth is under 300 mm, the particle's loading rate has no obvious law related to the barrel diameter. As the web depth increases, the proportion of particles in the statistical area first increases and then decreases with the increase in barrel diameter, which proves that loading rate of particles with a larger web depth can be effectively enhanced by increasing the barrel diameter to some extent.

From the comparison with Figure 15, the proportion of particles with a web depth of 600–750 mm significantly changed, which means that the loading effect of particles in this web depth is sensitive to the barrel diameter. This was followed by web depths of 450–600, 750–900 and 300–450 mm, and the particles with a web depth under 300 mm were

hardly affected by barrel diameter. It can be understood that the loading rate of particles with a web depth greater than 450 mm has an important impact on the drum's loading performance. Therefore, increasing the barrel diameter to a certain extent can effectively improve the loading rate of particles with a large web depth and further improve the drum's loading performance.
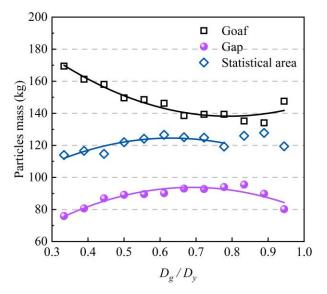

Figure 15. The effect of barrel diameter on conveying performance of particles with different web depths in ejection mode (D_y = 900 mm).

3.2. The Effect of Barrel on Coal-Loading Process under Pushing Conditions

3.2.1. The Distribution of Particles in Different Areas

The results of particles being distributed in different areas with pushing is shown in Figure 16. Similar to ejection, particle mass in the goaf first increases and then decreases with the increase in barrel diameter. The main difference is that its change range is notable when the barrel diameter is small, and the change is unnoticed with the increase in barrel diameter. Furthermore, the particles distributed in the gap area with pushing are different from those distributed with ejection. The barrel diameter almost has no impact on particle mass in gap area with ejection, while the particle mass in the gap area first increases and then decreases with the increase in barrel diameter with pushing. The main reason for this is that coal particles thrown by the helical vanes obtained a tangential velocity with ejection, thus obtaining a vertical upward velocity component, which weakened the natural falling caused by gravity and prolonged the ejection time, resulting in the particles being loaded onto the conveyor. The loading mechanism of pushing is different from that of ejection. Coal particles were excavated from the coal wall and piled up naturally on the floor and then were conveyed onto the conveyor using the blades' pushing action. When the barrel diameter is small, the particles piled up in the enveloping zone are inclined to slip to the goaf, resulting in a large mass in the goaf and a small mass in the gap area. As the barrel diameter increases, the capacity of the drum decreases and the interaction between drum and particles becomes complicated. This can be divided into two cases: (1) the filling rate of the drum half close to the coal wall is large, and the relative position of the particles and conveyor is high, making the particles more likely to cross the gap area over to the conveyor; (2) the input capacity decreases by half with the continuous increase in barrel diameter, and the particles overflow to the opposite half (conveying half of the drum with pushing) when the filling rate is too high, leading to a better conveying performance. Thus, the particle mass in the gap area decreases again when the barrel diameter continuously increases. It is noted that the particle mass in the statistical zone first increases and then decreases with the increase in barrel diameter. However, when the barrel diameter reaches
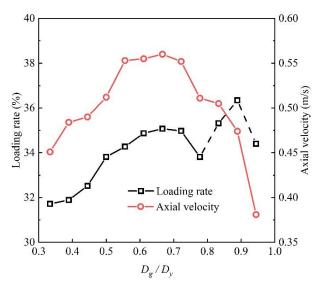
700 mm, with the continuous increase in the diameter, the particle mass in the loading zone does not continue to decline but increases again and then slowly decreases. The main reason for this phenomenon is similar to the above inference: when the barrel diameter is large, the distribution of particles in the goaf does not significantly increase but significantly decreases in the gap area, resulting in a temporary increase in the statistical zone.

Figure 16. The distribution of particles versus barrel diameter in pushing mode (D_y = 900 mm).

3.2.2. The Effect of Barrel Diameter on Particles' Loading Rate and Axial Velocities

The relationship between the coal-loading rate and particles' axial velocities with barrel diameter with pushing is shown in Figure 17. This can be described by a quadratic function: they first increase and then decrease with the increase in barrel diameter. When the D_g/D_y is 0.78, namely the barrel diameter is 700 mm, the changing trend of the loading rate is not consistent with the particles' axial velocities. As with the ejection mode, the particles' axial velocities continuously decrease with the increase in barrel diameter when the ratio of D_g/D_y exceeds 0.78, while the loading rate increases and then decreases, obtaining a peak with the 800 mm barrel diameter. The phenomenon is consistent with the above discussions, showing that the increment in barrel diameter causes more particles to cross the gap area onto the conveyor, leading the coal-loading rate to increase again.
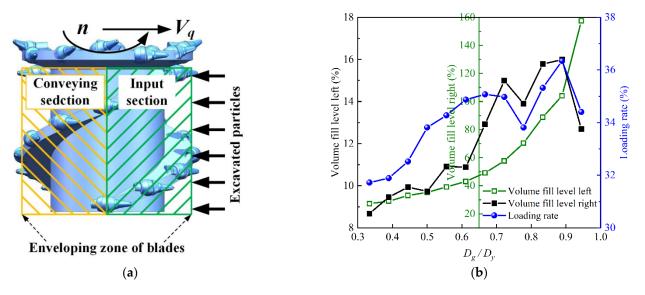

Figure 17. Loading rate and particles' axial velocities versus barrel diameter in pushing mode (D_y = 900 mm).

To verify the validation of the deduction, the filling rates of both drum halves was studied, as shown in Figure 18a. The relationships between the filling rate and loading rate and the conveying section and input section are shown in Figure 18b. The filling rate is given in Equation (3):

$$\eta_{fill} = \frac{M_{cc}/\rho}{V_c} \times 100\% \qquad (3)$$

where η_{fill} is the filling rate; M_{cc} is the particle mass in the enveloping zone; ρ is the accumulation density and V_c is the volume of the enveloping zone.
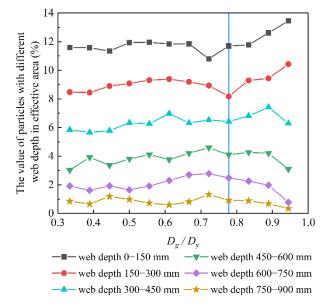

Figure 18. (**a**) Schematic diagram of input and conveying half under pushing conditions; (**b**) the relationship between filling rate and loading rate (D_y = 900 mm).

It can be seen from Figure 18a that the drum is evenly divided into two halves: the half close to the coal wall is the input section (right section), and the other is the conveying section (left section). It can be observed that the filling rate of the input half is greater than that of the conveying half in Figure 18b, due to the particles being excavated from the coal wall and accumulated in this half. Considering that the conveying capacity of the drum is constant for the changeless hauling and rotary speed, as the barrel diameter continuously increases, the space of the enveloping zone decreases, and the filling rate on the input half increases. Moreover, the change rules of the loading rate and filling rate on the conveying half with the barrel diameter are almost the same, especially when the barrel diameter is greater than 700 mm, which proves that the filling rate on the conveying half of the drum has an important impact on the loading rate. The results fully prove that the above inference is correct. According to the analysis of Figures 17 and 18b, when the barrel diameter is small, the main factor affecting the coal-loading performance of the drum is the particle axial velocities; when the barrel diameter continuously increases, the filling rate of particles inside the drum begins to play an important role.

3.2.3. The Effect of Barrel Diameter on Particles with Different Web Depths

The effect of barrel diameter on conveying the effect of particles with different web depths with pushing is shown in Figure 19. Similar to the ejection mode, when the particles are closer to the conveyor, the value in statistical area is higher. When the web depth is greater than 300 mm, the value of particles in the statistical area basically increases and then decreases with the increase in barrel diameter; when the web depth is lower than 300 mm, the variation law of the barrel diameter is less than 700 mm, consistent with web depth conditions of greater than 300 mm. When the barrel diameter exceeds 700 mm, particle values in statistical area increase continuously with the increasing barrel diameter. The reason for this result is consistent with the above discussion: larger barrel diameters enable

particles with a smaller web depth to have a relatively greater height at the end of the drum, which is conducive to crossing the gap area onto the conveyor. Hence, with Figure 17 it can be deduced that an increase in coal-loading rate when the barrel diameter exceeds 700 mm is caused by loading particles with less than 300 mm web depth.
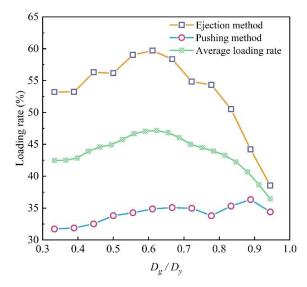

Figure 19. The effect of barrel diameter on conveying performance of particles with different web depths in pushing mode (D_y = 900 mm).

3.3. Comparison of Conveying Process under Ejection and Pushing Conditions

3.3.1. Comparison of Loading Rate under Ejection and Pushing Conditions

The comparison of loading rate under ejection and pushing conditions is shown in Figure 20. It can be observed that the coal-loading rate with ejection is larger than that of pushing, and the maximum difference exceeds 25%, consistent with Reference [32]. In addition, it is notable that the change in coal-loading rate with ejection is significantly higher than that with pushing. In comparison, the loading rate in pushing mode is less affected by the varying barrel diameter. The coal-loading rate with pushing is less affected by the barrel diameter, resulting in the change in the average drum loading rate, which is similar to the ejection rate, where the loading rate first increases and then decreases. The average loading rate of a 550–700 mm barrel diameter is more than 47.5%.
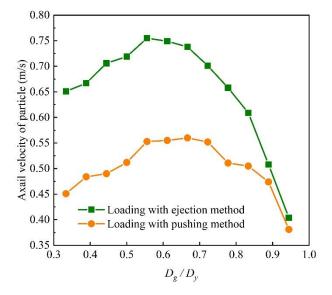

Figure 20. Comparison of loading rate under ejection and pushing conditions (D_y = 900 mm).

The main reason for the great difference in loading rate between the two loading modes is their different conveying mechanisms. With the ejection loading mode, both the input half and the conveying half of the loading drum are close to the coal wall. The particles that are cut off by the pick are directly affected by the spiral blades and allow the axial speed to flow in the direction of the scraper. As the conveying half is close to the coal wall, it is beneficial for the particles to stay in the enveloping zone during the conveying process. Meanwhile, particles at the end of the drum are subjected to the tangential ejection velocity of the blades to obtain a vertical upward velocity component, which is conducive to completing the loading across the gap area. Using the pushing mode, the conveying half and the input half are the two halves of the drum. The particles are intercepted in the enveloping zone of the blades and move in a circular motion into the conveying half under the tangential action of the blades. Since the rear side of the conveying half is the goaf area, the probability of particles being thrown into the goaf during conveyance increases, causing the conveying efficiency of the drum to decrease.

3.3.2. Comparison of Particles' Axial Velocities under Ejection and Pushing Conditions

The comparison of particles' axial velocities with different loading modes is shown in Figure 21. The variation laws of particles' axial velocities with the barrel diameter are consistent with the two loading modes. With the increase in barrel diameter, the particles' axial velocities first increase and then decrease. In addition, the particles' axial velocities with ejection are significantly higher than they are with pushing, especially when the barrel diameter is small. With pushing, the contact force between the particles clearly increases due to the push and extrusion of the blades; the collision is intense, and the kinetic energy of the particles is partially converted into internal energy, resulting in the particles' axial velocities being significantly less than they are in ejection.
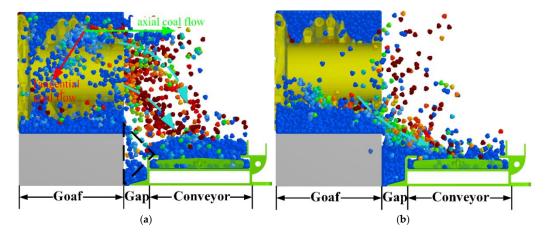

Figure 21. Comparison of particles' axial velocities under ejection and pushing conditions (D_y = 900 mm).

When the barrel diameter is small, the filling rate in the blade-enveloping zone is small, the distribution of particles in enveloping zone is dispersed and the transfer of contact force between particles and blades and between particles is not continuous. In addition, the filling rate in enveloping zone is small, the movement of particles in the blade enveloping zone is random and the probability of their being thrown out of the enveloping zone increases, resulting in small axial velocities.

With the increase in barrel diameter, the blade depth continuously decreases because the helical blade diameters are constant, and the action area acting on the particle flow is small in the conveying process. The subsequently intercepted particle flow obtains the axial velocity by relying on the force transmitted by the previous particle flow, and the

energy dissipation is caused by the transmission of contact force between particles; hence, the axial velocity of the subsequent particle flow decreases. In addition, as the diameter of the cylinder hub is too large, the internal capacity of the blades is small, and the contact between the particles and the barrel, the particles and the particle diameter is closer. The friction becomes an important factor in consuming particles' kinetic energy, resulting in a reduction in the axial velocity of the particles.

Figure 22 shows a diagram comparing the loading rate with different loading modes. At this time, the simulation time is 3.8 s, and the barrel diameter is 500 mm. Compared with (a) and (b) in Figure 22, it is obvious that the axial velocities of particles thrown from the drum with ejection are greater than those with pushing. Meanwhile, with ejection, the position of particles at the end of the drum is higher, so they can easily cross the gap area and load onto the conveyer, as discussed before. In comparison, with pushing, the position of particles at the end of the drum is too low, and a high number of particles accumulate in the gap area. After the stacking height reaches the edge height of the conveyor, some particles slide into the conveyor. The particles in the gap area accumulate at the end of the drum, which hinders the movement of subsequent particles, and is also the main reason for the small axial velocity of particles with pushing. In addition, the high accumulation of particles in the gap area is also unfavorable to the movement of the conveyor.

Figure 22. The comparison of coal-loading process in different loading modes: (**a**) ejection mode; (**b**) pushing mode.

3.3.3. Comparison of Conveying Performance for Particles with Different Web Depths under Ejection and Pushing Conditions

To further investigate the influence mechanism of loading modes on particles' conveying performance, the loading rates of particles with different web depths are obtained under ejection and pushing conditions, as shown in Figure 23. It can be seen from Figure 23 that the loading rate of particles in each web depth with ejection is greater than that with pushing, and as mentioned previously, there is no obvious law for the change in particle loading rate with barrel diameter with the two loading modes when the wen depth is small (0–300 mm). With the increase in web depth, the barrel diameter shows an obvious regularity for particles' loading rate. In addition, it can be seen from Figure 23 that the dispersion of particle loading rate with ejection is significantly greater than that with pushing, which further proves that the particle loading rate is more affected by the barrel diameter with ejection. In addition, statistics show the difference in particles' average loading rate at different web depths, caused by the loading mode in the simulation, as shown in Table 2. The statistical results in Table 2 are plotted in Figure 13. Table 2 and Figure 24 show that the difference in average loading rate with the two different loading modes first increases and then decreases with the increase in web depth. The largest difference was seen for the particles with web depths of 450–600 and 300–450 mm. The ejection mode was 4.150% and 4.044% higher than the pushing mode. The second largest difference was seen for the

section depths of 150–300, 600–750 and 750–900 mm. The minimum impact was seen for the section depth of 0–150 mm, with a difference of 1.952%. This proves that the loading mode has a great influence on the conveying rate of particles in the middle of the coal wall but has no obvious influence on the particles at both ends, i.e., at the end plate and near the conveyor. In addition, the particles (0–300 mm) with a small web depth with pushing are greatly affected by the change in barrel diameter, and the effect of barrel diameter with ejection is not obvious. With the increase in web depth, the particle loading rate with ejection is obviously affected by the change in barrel diameter. However, the particle loading rate with pushing changed little with the change in barrel diameter.
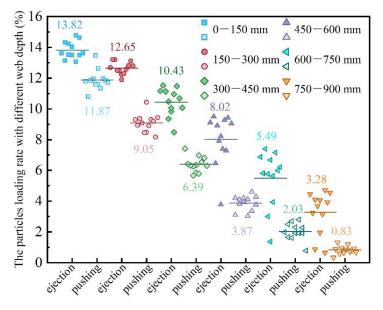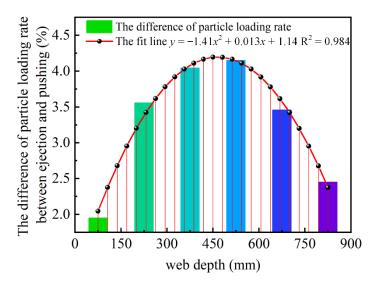

Figure 23. Loading rate of particles with different web depths.

Table 2. The statistical results of differences in loading rate for particles with different web depths under ejection and pushing conditions.

Web Depth/mm	0–150	150–300	300–450	450–600	600–750	750–900
Difference of loading rate/%	1.952	3.558	4.044	4.150	3.458	2.449

Figure 24. The difference in loading rate for particles with different web depths under ejection and pushing conditions.

4. Conclusions

To study the influence of barrel diameter on coal-loading rate during the conveying process, the pivotal parameters of particles using the discrete element method were calibrated through experiments. Secondly, the validity of the developed DEM model was experimentally verified by the drum loading test. Finally, with the help of the DEM, the effects of the barrel diameter on particles' axial velocities, the distribution of particles, the loading rate of particles with different web depths and different loading modes were studied, and the action mechanism of the barrel diameter in the loading process is further revealed. The main conclusions of this paper are as follows:

(1) Using the ejection mode, the particle loading rate is clearly affected by the particles' axial velocities. With the increase in barrel diameter, this first increases and then decreases, and the best coal-loading rate is obtained with the barrel diameter in the range of 500 to 600 mm. The barrel's influence on the particles' loading rate with a small web depth (0–300 mm) is not obvious. With the increase in web depth, the variation law of particle loading rate with the barrel diameter in each area is consistent with that of the coal-loading rate.

(2) Using pushing mode, the loading rate of the drum is mainly affected by the particles' axial velocity and the filling rate: when the barrel diameter is small, the loading rate is more significantly affected by the particles' axial velocity. With the increase in the barrel diameter, when the diameter ratio of the barrel to the helical blades is greater than 0.78, the particle filling rate in the enveloping zone has an obvious effect on the loading rate.

(3) The influence mechanism of a barrel diameter with ejection and pushing is different. The axial velocity and loading rate of particles with ejection are greater than those with pushing, especially when the barrel diameter is small. Compared with the pushing mode, the coal-loading rate with ejection is increased by about 25%, and the axial velocity of particles is increased by about 50%. The difference in coal-loading rate between ejection and pushing is mainly affected by the particle loading rate within the web depth of 300–600 mm, and the loading mode has no obvious effect on the particle loading rate at the end plate and near the conveyor. The effect of barrel diameter on drum loading rate is more obvious using ejection but not pushing mode.

Author Contributions: Conceptualization, X.Z., K.G. and Q.Z.; methodology, X.Z.; software, T.W. and L.L.; validation, Q.Z. and L.S.; formal analysis, X.Z.; investigation, K.G.; resources, K.G.; data curation, X.Z.; writing—original draft preparation, X.Z. and K.G.; writing—review and editing, Q.Z.; visualization, X.Z.; supervision, K.G.; project administration, K.G.; funding acquisition, K.G. All authors have read and agreed to the published version of the manuscript.

Institutional Review Board Statement: Not applicable.

Informed Consent Statement: Not applicable.

Data Availability Statement: Not applicable.

Conflicts of Interest: The authors declare no conflict of interest.

References

1. Wang, Q.; Song, X.; Liu, Y. China's coal consumption in a globalizing world: Insights from Multi-Regional Input-Output and structural decomposition analysis. *Sci. Total Environ.* **2020**, *711*, 134790. [CrossRef] [PubMed]
2. Wan, L.; Jiang, K.; Gao, K.; Zeng, Q.; Zhang, X. Research of response difference on coal cutting load under different cutting parameters. *Stroj. Vestn. J. Mech. Eng.* **2019**, *65*, 420–429. [CrossRef]
3. Eshaghian, O.; Hoseinie, S.H.; Maleki, A. Multi-attribute failure analysis of coal cutting picks on longwall shearer machine. *Eng. Fail. Anal.* **2021**, *120*, 105069. [CrossRef]
4. Li, X.; Wang, S.; Ge, S.; Malekian, R.; Li, Z.; Li, Y. A study on drum cutting properties with full-scale experiments and numerical simulations. *Meas. J. Int. Meas. Confed.* **2018**, *114*, 25–36. [CrossRef]
5. Ma, D.; Zhang, X.; Wan, L.; Zeng, Q.; Ge, H. Dynamic analysis of shearer traction unit considering the longitudinal swing. *Energies* **2020**, *13*, 5293. [CrossRef]
6. Wan, L.; Ma, D.; Zhang, X. Research on Meshing Characteristics of Shearer Walking Wheel Based on Rigid-Flexible Coupling. *Math. Probl. Eng.* **2020**, *2020*, 8301086. [CrossRef]
7. Kotwica, K.; Stopka, G.; Gospodarczyk, P. Simulation tests of new solution of the longwall shearer haulage system. *IOP Conf. Ser. Mater. Sci. Eng.* **2019**, *679*, 012002. [CrossRef]
8. Gospodarczyk, P. Modeling and Simulation of Coal Loading by Cutting Drum in Flat Seams. *Arch. Min. Sci.* **2016**, *61*, 365–379. [CrossRef]
9. Tian, Z.; Jing, S.; Zhao, L.; Liu, W.; Gao, S. Numerical simulation on coal loading process of shearer drum based on discrete element method. *Energy Explor. Exploit.* **2021**, *36*, 1919–1938. [CrossRef]
10. Gao, K. *Study on Coal Loading Performance of Thin Coal Seam Shearer*; China University of Mining & Technology: Xuzhou, China, 2014.
11. Ayhan, M. *Investigation into the Cutting and Loading Performance of Drum Sheaerer in OAL Mine*; The University of Hacettepe: Ankara, Turkey, 1994.
12. Bołoz, Ł. Unique project of single-cutting head longwall shearer used for thin coal seams exploitation. *Arch. Min. Sci.* **2013**, *58*, 1057–1070. [CrossRef]
13. Gao, K.; Zhang, X.; Jiang, K.; Yang, Y.; Yin, G.; Liu, B. An Applied Model of Minimum Rotating Speed for Drum Shearer to Avoid Drum Clogging. *J. Eng. Res.* **2019**, *7*, 1–19. [CrossRef]
14. Wydro, T. Influence of the plow filling and thread angle onto the plow head efficiency. *Arch. Min. Sci.* **2015**, *60*, 143–156. [CrossRef]
15. Cundall, P.A.; Strack, O.D.L. A discrete numerical model for granular assemblies. *Geotechnique* **1979**, *29*, 47–65. [CrossRef]
16. López, A.; Vivacqua, V.; Hammond, R.; Ghadiri, M. Analysis of screw feeding of faceted particles by discrete element method. *Powder Technol.* **2020**, *367*, 474–486. [CrossRef]
17. Wang, S.; Li, H.; Tian, R.; Wang, R.; Wang, X.; Sun, Q.; Fan, J. Numerical simulation of particle flow behavior in a screw conveyor using the discrete element method. *Particuology* **2019**, *43*, 137–148. [CrossRef]
18. Wang, S.; Ji, Y.; Wang, S.; Chen, Y.; Tian, R.; Ma, Y.; Sun, Q. Comparison of computational fluid dynamics–discrete element method and discrete element method simulations for a screw conveyor. *Asia-Pac. J. Chem. Eng.* **2020**, *15*, e2394. [CrossRef]
19. Han, Y.; Jia, F.; Zeng, Y.; Jiang, L.; Zhang, Y.; Cao, B. DEM study of particle conveying in a feed screw section of vertical rice mill. *Powder Technol.* **2017**, *311*, 213–225. [CrossRef]
20. Yang, D.; Wang, Y.; Li, J.; Wang, Q.; Wang, Y.; Yu, Y. Simulation study on interaction coefficient of DEM in non–spherical large size (5–30 mm) coal particles. *Particuology* **2020**, *53*, 142–153. [CrossRef]
21. Yang, D.; Li, G.; Wang, Y.; Wang, Q.; Li, J.; Huang, Q.; Xia, Y.; Li, Q. Prediction of Horizontal Pneumatic Conveying of Large Coal Particles Using Discrete Phase Model. *Adv. Mater. Sci. Eng.* **2020**, *2020*, 1967052. [CrossRef]
22. Yang, D.; Xing, B.; Li, J.; Wang, Y.; Hu, N.; Jiang, S. Experiment and simulation analysis of the suspension behavior of large (5–30 mm) nonspherical particles in vertical pneumatic conveying. *Powder Technol.* **2019**, *354*, 442–455. [CrossRef]
23. Li, K.; Kuang, S.B.; Pan, R.H.; Yu, A.B. Numerical study of horizontal pneumatic conveying: Effect of material properties. *Powder Technol.* **2014**, *251*, 15–24. [CrossRef]
24. Zhou, M.; Kuang, S.; Luo, K.; Zou, R.; Wang, S.; Yu, A. Modeling and analysis of flow regimes in hydraulic conveying of coarse particles. *Powder Technol.* **2020**, *373*, 543–554. [CrossRef]
25. Kuang, S.; Zhou, M.; Yu, A. CFD-DEM modelling and simulation of pneumatic conveying: A review. *Powder Technol.* **2020**, *365*, 186–207. [CrossRef]
26. Takabatake, K.; Mori, Y.; Khinast, J.G.; Sakai, M. Numerical investigation of a coarse-grain discrete element method in solid mixing in a spouted bed. *Chem. Eng. J.* **2018**, *346*, 416–426. [CrossRef]
27. Van Wyk, G.; Els, D.N.J.; Akdogan, G.; Bradshaw, S.M.; Sacks, N. Discrete element simulation of tribological interactions in rock cutting. *Int. J. Rock Mech. Min. Sci.* **2014**, *65*, 8–19. [CrossRef]
28. Su, O.; Ali Akcin, N. Numerical simulation of rock cutting using the discrete element method. *Int. J. Rock Mech. Min. Sci.* **2011**, *48*, 434–442. [CrossRef]
29. Xuefeng, L.; Shibo, W.; Shirong, G.; Malekian, R.; Zhixiong, L. Investigation on the influence mechanism of rock brittleness on rock fragmentation and cutting performance by discrete element method. *Meas. J. Int. Meas. Confed.* **2018**, *113*, 120–130. [CrossRef]

30. Gao, K.; Wang, L.; Du, C.; Li, J.; Dong, J. Research on the effect of dip angle in mining direction on drum loading performance: A discrete element method. *Int. J. Adv. Manuf. Technol.* **2017**, *89*, 2323–2334. [CrossRef]
31. Gao, K. Feasibility of drum coal loading process simulation using three-dimension discrete element method. *Eletron. J. Geotech. Eng.* **2015**, *20*, 5999–6007.
32. Gao, K.; Zhang, X.; Sun, L.; Zeng, Q.; Jiang, K. Complex Effects of Drum Hub Forms and Structural Parameters on Coal Loading Performance. *Complexity* **2020**, *2020*, 7036087. [CrossRef]
33. Sun, L.; Zhang, X.; Zeng, Q.; Gao, K.; Jiang, K.; Zhou, J. Application of a screw conveyor with axial tilt blades on a shearer drum and investigation of conveying performance based on DEM. *Particuology* **2021**, *61*, 91–102. [CrossRef]
34. Potyondy, D.O.; Cundall, P.A. A bonded-particle model for rock. *Int. J. Rock Mech. Min. Sci.* **2004**, *41*, 1329–1364. [CrossRef]
35. Coetzee, C. Calibration of the discrete element method: Strategies for spherical and non-spherical particles. *Powder Technol.* **2020**, *364*, 851–878. [CrossRef]
36. Coetzee, C.J. Review: Calibration of the discrete element method. *Powder Technol.* **2017**, *310*, 104–142. [CrossRef]
37. Fu, L.; Wang, K.; Hu, B.; van Xo, N. Conveying performance of drilling tool of auger miner at different strike angles based on discrete element method. *Powder Technol.* **2021**, *378*, 202–215. [CrossRef]
38. Fu, L. Study on Cutting and Conveying Performance of Novel Auger Miner Drilling Tool. Ph.D. Thesis, China University of Mining and Technology, Xuzhou, China, 2016.